# First observation of thermal ion internal transport barrier on the HL-2A tokamak

D.L. Yu, Y. L. Wei, L. Liu, J. Y. Cao, A. P. Sun, Z. B. Shi, B.S. Yuan, W. J. Chen, Q. Ma, X. X. He, K.J. Zhao, X.Q. Ji, Y. Zhou, M. Jiang, W. L. Zhong, W. Deng, Y.G. Li, J.M. Gao, Yi Liu, Y. Xu, L. W. Yan, Q. W. Yang, X. T. Ding, J.Q. Dong, X. R. Duan, Yong Liu and HL-2A team

*Southwestern Institute of Physics, Chengdu, China*

The peaked density and temperature plasma is always pursued as it ensures the possibility of an operating merits characterized by high beta, high energy confinement time, and a large fraction of bootstrap current. The discharge with the internal transport barriers (ITBs), which origins from the pellet injection experiments [1], is a promising regime to satisfy the demand. The previous investigation reveals that the reversed (weak) magnetic shear is very important to develop the ITBs [2]. On ASDEX-U and JET tokamaks, the q = 1 ITB characteristics are compared [3]. Both of them are accompanied the fishbone oscillations, the q profiles are rather flat in the plasma core. The fishbone and the long lasting mode (LLM) are observed during the NBI heating on HL-2A tokamak. They are driven by the energetic particles in tokamaks; the former is a typical internal kink mode [4], and the latter is internal kink-like mode [5]. The appearance of these modes indicates the q profiles in the core are weakly or reversely sheared [5]. Recently, a 32/64-channel charge exchange recombination spectroscopy (CXRS) diagnostic system is developed on the HL-2A tokamak (R = 1.65 m, a = 0.4 m), monitoring plasma ion temperature and toroidal rotation velocity simultaneously with spatial and temporal resolutions up to ~1 cm and 5 ms [6, 7]. And the ion ITBs are observed during the NBI heating. Besides, a 32-channel fast electron cyclotron emission (ECE) system can provide the electron temperature ($T_e$) with temporal and spatial resolutions up to 0.8 μs and 1 cm[8].

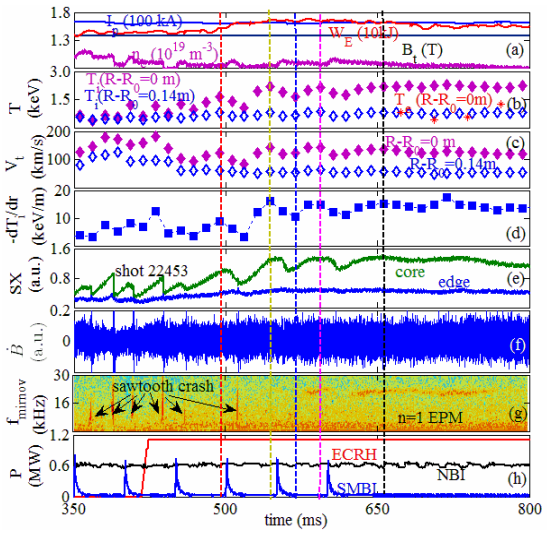


Figure 1. Typical ITB discharge on HL-2A

In shot 22453, the powers of neutral

beam injection (NBI) and ECRH are about 0.6 MW and 1.1 MW, respectively; the line-averaged plasma density is 0.8~0.9 $\times 10^{19}$ $m^{-3}$, as shown in figure 1(a). The ion temperature in the core $T_i(0)$ is slightly higher than $T_i(r/a = 0.37)$ before 490 ms, indicating that the gradient in the core is small; however, the gradient becomes steeper at around 500 ms, and $T_i(0)$ is three times as high as that of $T_i(r/a = 0.37)$, whereas the core electron temperature $T_e(0)$ is the same as the $T_i$ at r/a = 0.37, as shown in figure 1(b); the sawtooth oscillation disappeared after 512 ms. The energetic particle mode (n = 1) can be observed after 570 ms, as shown in figure 1(g). Meanwhile, the stored plasma energy is increased when the ion temperature gradient

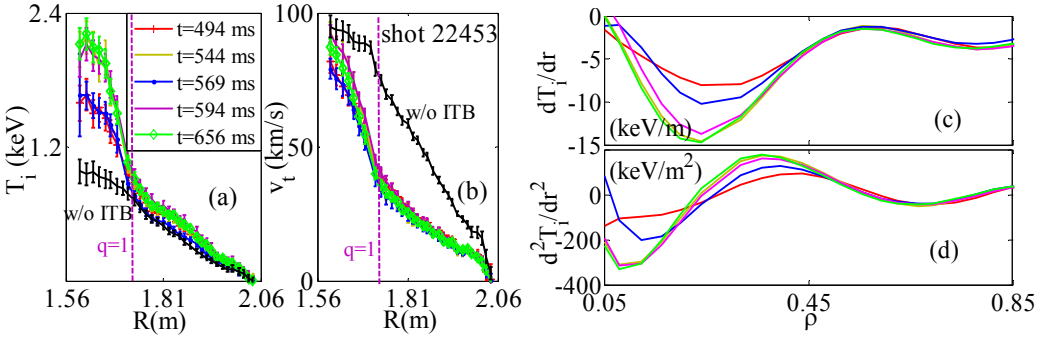


Figure 2. $T_i$ (a) and $v_t$ (b) profiles and the first (c) and second (d) derivative of Ti.

becomes steeper, as shown in figures 1(a) and (d). It is observed that the $T_i$ and $v_t$ are peaked after the increase of stored energy, as shown in figure 2 (a) and (b). The $T_i$ during the stored energy increase (t = 494 ms) is similar to that after the SMBI pulse (t = 569 ms), as shown in figure 2(a); and it is clearly lower than those of other time, as the former is not well developed and the latter is influenced by the SMBI. Furthermore, the first and second derivative of ion temperature is analyzed, as shown in figure 2(c) and (d). The first derivative of ion temperature can be up to -15 keV/m, and it is about -10 ~ -7 keV/m for the sawtooth and during the SMBI phases, respectively. The maximum second derivative of ion temperature can be up to 175 keV/$m^2$, this value decreases to 2/3 and 1/2 after SMBI and during the sawtooth phases, respectively. For the

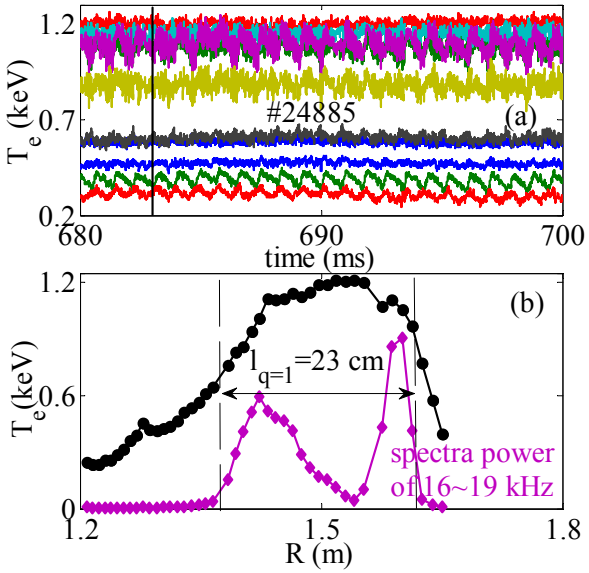


Figure 3. The position of ITB foot. Time traces of the $T_e$ (a) and the radial profiles (b).

second derivative of ion temperature, there exist two extrema, one locates at the foot of the peaked ion temperature and the other is close to the plasma core.

According to the ion temperature profiles, the ITB foot is around ~ 12~14 cm away from the plasma core. The location of the ITB foot is a key parameter to understand the mechanisms and the formation of the ITB. Therefore, it is necessary to obtain the location from other plasma parameters. The 32-channel ECE system has the spatial resolution of 1~2 cm. The time evolution of the $T_e$ and the radial profiles are shown in figure 3(a) and (b), respectively. The n = 1 LLM can be observed in the soft x-ray arrays, ECE system and Mirnov coils. To determine the q = 1 surface, the ECE signals are filtered and the radial profile of the spectrum power of 16~19 kHz can be obtained, as shown in figure 3(b). As the LLM is an internal-kink-like mode, they decrease sharply close to q=1 surface, therefore, the q = 1 surfaces are determined by the e-fold decay of the maximum intensity. And the averaged r = 11.5 cm of q=1 surface can be derived. It is about 2~3 cm smaller than the CXRS due to the spatial resolution is around ~3 cm in the plasma core.

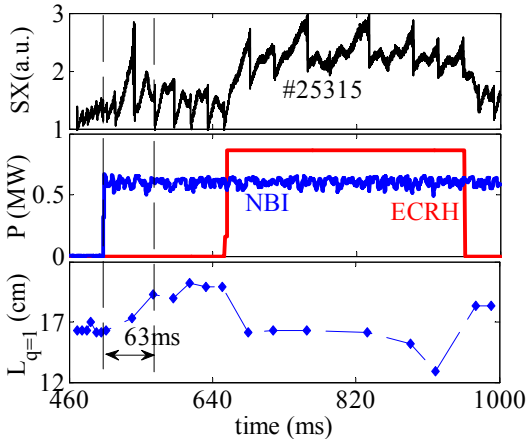


Figure 4. Time traces of soft X-ray(a), power of NBI and ECRH(b), the width of q=1(c).

The reason of ITB tending to be formed at the beginning of the NBI is due to the current drive effect of the NBI. As the motional Stark effect polarimeter is not available, the current drive effect of NBI is verified by the width of q = 1 measured by the ECE system during the sawtooth crash. The $L_{q=1}$ is defined as the width between the q=1 surfaces at high field and low field sides. For shot 25315, the $L_{q=1}$ is around 16 cm during the Ohmic phase, and is increased to ~20 cm during the NBI heating; the width is decreased to the Ohmic level during the ECRH and NBI phase; and when the ECRH is switched off, the width is again increased to ~20 cm. This experiment indicates that the NBI can increase the $L_{q=1}$ and hence the weak shear of the q profiles are available. Another reason for the ITB formation may relay on the plasma rotation shear at the beginning of the NBI heating phase. The plasma rotation is anti-current direction at first; and the direction changes due to the input torque from the NBI. On the other hand, the NBI torque deposit more in the core than that at the edge, therefore, the increase in the core is much evident and hence the velocity shear can be observed at the vicinity of q=1 surface.

The normalized ion temperature gradient ($R/L_{Ti}$) is compared for 17 shots, as shown in figure 5. For the ITB shots 22453, 24885, 24887, 24889, 24893, 25092 and 25099 etc., the $R/L_{Ti}$ is clearly higher; among these shots, the long lasting modes (fishbone oscillations) are observed during the peaked ion temperature and velocity. For shots 22865 and 22870, sawtooth and short duration fishbone oscillations are observed during the peaked phases. Another interesting phenomenon is that the $T_i(0.5)$ of the discharges without the ITBs seems not lower than that with the ITBs. Further analysis indicates that they are decreased with the maximum value of normalized ion temperature gradient inside the ITB. The $R/L_{Ti}$ at the r/a = 0.5 has the same trend with $T_i(0.5)$, indicating that better confinement inside the ITB will result in worse confinement outside it. However, the mechanism is unknown. In other words, it is easy to understand that the $T_i(0)$ is higher when the confinement becomes better, but the trend for $T_i(0.5)$ is not the case.

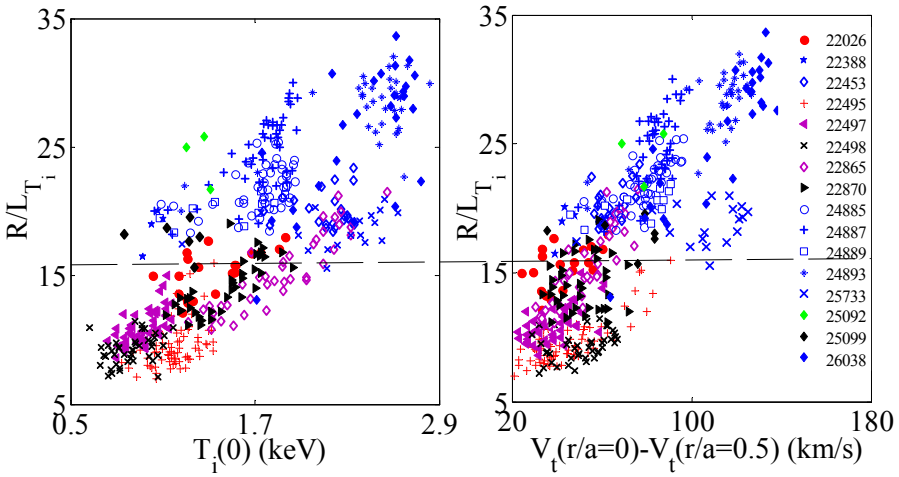


Figure 5. The $R/L_{Ti}$ versus $T_i(0)$ (a) and $v_T(0)$ (b).

The thermal ion internal transport barriers are firstly observed during the neutral beam injection (NBI) on the HL-2A tokamak. The ITBs are accompanied with the long-lasting mode, and the position of the barrier foot is at the q = 1 surface. The ITB can be more frequently observed at the beginning of the NBI heating due to the current drive effect.

## References

[1] A. Weller *et al*., Physics Review Letters **59** 2303(1987).
[2] M. Hugon *et al*., Nuclear Fusion **32** 33 (1992).
[3] E. Joffrin *et al*., Plasma Physic and Controlled Fusion **44** 1203 (2002).
[4] G.Y. Fu *et al*., Physics of Plasmas **13** 052517 (2006).
[5] R. B. Zhang *et al*., Plasma Physic and Controlled Fusion **56** 095007 (2014).
[6] D.L. Yu *et al*., Review Scientific Instruments **85** 11E402 (2014).
[7] Y. L. Wei *et al*., Review Scientific Instruments **85** 103503 (2014).
[8] Z.B. Shi *et al*., Review Scientific Instruments **85** 023510 (2014).